AIChE

The Potential of Current High-Resolution Imaging-Based Particle Size Distribution Measurements for Crystallization Monitoring

P. A. Larsen and J. B. Rawlings
Dept. of Chemical and Biological Engineering, University of Wisconsin-Madison, Madison, WI 53706

DOI 10.1002/aic.11739

High-speed, in situ video microscopy is a promising technology for measuring critical solid-phase properties in suspension crystallization processes. This paper demonstrates the feasibility of high-resolution, video-imaging-based particle size distribution (PSD) measurement by applying image analysis and statistical estimation tools to images from a simulated batch crystallization of an industrial photochemical. The results also demonstrate the ability to monitor important quality parameters, such as the ratio of nuclei mass to seed mass, that cannot be monitored by conventional technologies. General recommendations are given for achieving appropriate sampling conditions to enable effective imaging-based PSD measurement. © 2009 American Institute of Chemical Engineers *AIChE J,* 55: 896–905, 2009

Keywords: crystallization, image analysis, imaging, particle size distribution, pharmaceuticals, process monitoring

Introduction

Solution crystallization is a commonly used but often poorly controlled process for separating or purifying chemical species in the pharmaceutical, chemical, and food industries. The development of effective solid-phase monitoring technology is a critical step to enable better understanding and control of crystallization processes. Video imaging is a promising technology offering the potential to monitor critical solid-phase properties, including particle size distribution (PSD), shape distribution, and, in some cases, polymorphic fraction. For example, in situ video imaging is used by Schöll et al.[1] to observe the solvent-mediated polymorphic transformation of L-glutamic acid from the α form with prismatic morphology to the β form with a needle-like morphology. Monnier et al.[2] used off-line image analysis to characterize the final relative PSD of adipic acid crystals. Pöllänen et al.[3] used video microscopy and automated image analysis to characterize the sizes and shapes of sulphathiazole crystals. The application of video imaging to these crystallization processes, however, is limited to qualitative monitoring or characterization of end-product properties.

Only a few studies have used video imaging for on-line, quantitative monitoring of crystal population dynamics. Patience et al.[4] used video microscopy to monitor the evolution of crystal size mean and standard deviation for needle-like pharmaceutical particles. The slurry was sampled periodically and allowed to settle on a microscope stage, and the images were analyzed manually. Calderon de Anda et al.[5] used noninvasive imaging and automatic image analysis to quantify the polymorphic fraction during the transformation from α to β L-glutamic acid. In a follow-up study, Dharmayat et al.[6] monitored on-line the L-glutamic acid transformation using both on-line video microscopy and X-ray diffraction, but were unable to compare quantitatively the measurements of the two methods because the video microscopy technique

---

Correspondence concerning this article should be addressed to J. B. Rawlings at rawlings@engr.wisc.edu.

failed at higher solids concentrations, and the X-ray diffraction method was not sufficiently sensitive at low solids concentrations. Larsen et al.[7] developed an image analysis algorithm to segment in situ images of rod-like particles and compared the cumulative distribution function (CDF) measured by their algorithm with the CDF obtained by manual image analysis. The comparison was made using four different sets of images acquired at 50–100 min intervals during a pharmaceutical crystallization. Larsen et al.[8] carried out a similar study for particles having complex shapes that can be represented by a wireframe model. Qu et al.[9] used in-line imaging to monitor the evolution of crystal length and width CDFs at 10–20 min intervals, determining width and length growth rates based on the mean particle size.

Besides these crystallization applications, video imaging has been used to monitor dynamics of other particulate processes. Watano and Miyanami[10] demonstrated on-line monitoring of the median diameter and shape factor for a wet granulation process using in situ video imaging and automatic image analysis. Blandin et al.[11] used noninvasive imaging of an agglomeration process and automatic image analysis to track the evolution of the particle size number fractions at 30-min intervals for about 4 h. They validated their automated image analysis method using comparisons with manual image analysis. Hukkanen et al.[12] used in situ video microscopy and automated image analysis to monitor various PSD moments during the early stages of a suspension polymerization processes.

In summary, the imaging-based, particulate population dynamics studies in the literature have focused on monitoring the CDF, the normalized PSD (i.e., number fraction), moments of the PSD (e.g., mean size and variance), or polymorphic fraction. Given that the dynamics of particle populations are modeled in terms of the absolute PSD, it is desirable to monitor the absolute PSD to enable better model identification and control.

Imaging-based PSD measurement involves various challenges. One of the key challenges is achieving robust image analysis. Image analysis is most effective for images having high contrast, sharp focus, and minimal particle overlap. Successful imaging-based measurement, therefore, depends not only on the optical properties of the imaging system, but also on the solids concentration, the sizes and shapes of the particles, and the tendency of the particles to agglomerate or floc together. The presence of both large and small particles in crystallization processes presents challenges for optical system design as well as image analysis. The optical system must not only have high resolution to track the small particles but also a large field of view to track the large particles. As resolution increases, both the field of view and depth of field decrease. Although the decrease in depth of field simplifies image analysis by enabling discrimination between overlapping particles, it also reduces the number of measurements obtained in a single image, leading to sampling concerns that cannot be overcome simply by increasing the video camera frame rate. Obtaining independent samples requires that each frame contain a new population of crystals. In other words, the accuracy of the PSD measurement is not improved by resampling the same subpopulation of crystals.

Extracting the PSD from video images requires not only suitable image analysis and optical design but also statistical estimation to correct for sampling biases inherent in imaging-based measurement. Larsen and Rawlings[13] derived a maximum likelihood estimator (MLE) of the PSD that corrects sampling bias due to the finite size of the imaging window, enabling unbiased estimation of the PSD as well as quantification of measurement uncertainty. The estimator assumes that image analysis is perfect, or that every particle in the image is identified correctly. Noting that perfect image analysis is a reasonable assumption only for low solids concentrations, Larsen and Rawlings[14] also developed a method for estimating the number density of monodisperse particle populations at high solids concentrations with heavy particle overlap and imperfect image analysis. The effectiveness of these tools was demonstrated, however, using artificial images generated at stationary process and imaging conditions. The objective of this study is to demonstrate the feasibility of imaging-based PSD measurement for realistic and changing process and imaging conditions. We achieve this objective by simulating a well-studied industrial crystallization process and generating images of the process based on the specifications of a commercially available in situ imaging probe. Furthermore, this study shows the value of imaging-based measurement by demonstrating the measurement of process properties that cannot be measured by conventional technologies.

Although the images used in this study are idealized, the relevant camera specifications (i.e., resolution, magnification, field of view, sampling rate) reflect current camera hardware. By using idealized images, the study assesses the *limits* of what can be inferred using current camera hardware in the environment of a crystallizer operating at realistic nucleation and growth rates.

The article is outlined as follows. The Simulation Methods section describes the crystallizer model used in this study and the method for generating images corresponding to the current state of the crystallizer. The Results and Discussion section presents the simulation results, demonstrating the measurement of important product–quality metrics and multimodal PSDs. This section also offers general guidelines for designing imaging based PSD monitoring systems. The Conclusions section summarizes our conclusions and suggests areas for further research.

Simulation Methods

Crystallizer model and solution

Batch crystallization can be modeled using a system of partial integro-differential equations that couples mass and energy balances with a population balance describing the evolution of the crystal population's PSD. The population balance used in this study is

$$\frac{\partial f}{\partial t} + G\frac{\partial f}{\partial L} = 0 \tag{1}$$

in which $f(L, t)$ is the PSD, L is the characteristic length, and G is the crystal growth rate. The boundary condition is

$$f(0,t) = \frac{B^{\circ}}{G(L=0)} \tag{2}$$

in which B° is the nucleation rate density. G and B° depend on the relative supersaturation S and are assumed to follow standard semiempirical power laws:

$$S = \frac{\hat{C} - \hat{C}_{\text{sat}}}{\hat{C}_{\text{sat}}} \quad G = k_g S^g \quad B^\circ = k_b S^b \mu_3^j \tag{3}$$

in which $\hat{C}$ is the liquid-phase solute concentration, $\hat{C}_{\text{sat}}$ is the saturation concentration, k_g and g are growth rate constants, and k_b, b, and j are nucleation rate constants. The ith moment of the PSD, μ_i, is defined as

$$\mu_i = \int_0^\infty f L^i dL \tag{4}$$

In this study, we also are concerned with moments corresponding to subsets of the total crystal population. Moments corresponding to crystals grown from nuclei are denoted with a subscript N (e.g., μ_{N_3}) whereas moments corresponding to crystals grown from seeds are denoted with a subscript S.

Assuming, as above, that growth rate is size independent and the system is closed (no input or output streams), the mass balance for the solute concentration is

$$\frac{d\hat{C}}{dt} = -3\rho_c k_v h G \int_0^\infty f L^2 dL \tag{5}$$

in which $\hat{C}$ is the solute concentration, ρ_c is the crystal density, k_v is a shape factor defined such that $k_v L^3$ gives the volume of a crystal of characteristic length L, and h converts solvent mass to slurry volume. $\hat{C}$ is given in terms of mass of solute per total mass of solution or liquid phase. The initial condition is given by $\hat{C} = \hat{C}_0$.

For the simulations used in this study, the energy balance is unnecessary as we assume perfect temperature control. The temperature follows a fixed temperature trajectory without deviation.

The model parameters used in this study correspond to a well-studied, industrial photochemical crystallization process.[15,16] The parameters for this process are given in Table 1. The particles have a plate-like morphology and the characteristic length corresponds to the particle width. A height-to-width ratio of 10 and a width-to-depth ratio of 4 are assumed. The seed mass is 0.1 g and the seed population is assumed to have a parabolic form with a minimum characteristic length of 0 and maximum characteristic length of 10, corresponding to primary axis lengths of 0 and 100, respectively. The saturation concentration $\hat{C}_{\text{sat}}$ for this system is given by

$$\hat{C}_{\text{sat}}(T) = 0.185 - 2.11 \times 10^{-2} T + 7.46 \times 10^{-4} T^2 \tag{6}$$

Table 1. Parameters Used to Simulate Industrial Batch Crystallization Process of Photochemical[15]

Description	Symbol	Value	Units
Kinetic growth rate constant	k_g	0.3e-4	cm/min
Power-law exponent	g	2.0	dimensionless
Kinetic nucleation rate constant	k_b	2.6e10	g solvent/cm^3 min
Power-law exponent	b	3.0	dimensionless
Moment exponent	j	2.0	dimensionless
Crystal density	ρ_c	1.183	g/cm^3
Volumetric shape factor	k_v	2.5	dimensionless
Crystallizer volume	V	2.3	L
Initial solute concentration	$\hat{C}_0$	0.11	g solute/g solvent

The characteristic length is the particle width. A constant aspect ratio (AR) of 10 is assumed along with a constant width-to-depth ratio of 4.

The percent volume of solids reaches approximately 2.5%. The crystallizer model is solved using orthogonal collocation on moving finite elements. The method is described in detail elsewhere.[17]

Artificial image generation

To generate an artificial image, we simulate the particle population in a local region surrounding the imaging volume V_I. In this region, we model the particle population as a three-dimensional stochastic process $\Phi = (\mathbf{X}_{wi}, L_i, \Theta_{zi})$ on $\mathbb{R}^3 \times \mathbb{R}^+ \times (-\pi/2, \pi/2]$ for $i = 1, \ldots, \tilde{N}_c$. $\mathbf{X}_{wi} = (X_{wi}, Y_{wi}, Z_{wi})$ gives the location of the centroid for particle i in the world coordinate frame, L_i gives the particle characteristic length, Θ_{zi} gives the orientation around the z-axis of the world coordinate frame, and $\tilde{N}_c$ gives the number of particles. $\mathbf{X}_{wi}$, L_i, Θ_{zi}, and $\tilde{N}_c$ are distributed independently of each other. X_{wi}, Y_{wi}, Z_{wi}, and Θ_{zi} are distributed uniformly on $[x_{\min}, x_{\max}]$, $[y_{\min}, y_{\max}]$, $[z_{\min}, z_{\max}]$, and $(-\pi/2, \pi/2]$, respectively. L_i has a cumulative distribution function given by

$$H(L) = \begin{cases} 0 & L \le R \\ \int_R^L f(l)dl / \int_R^{L_{\max}} f(l)dl & R < L \le L_{\max} \\ 1 & L > L_{\max} \end{cases}$$

in which R is the lower limit of resolution of the camera and $L_{\max}$ is defined as the size of the largest particle in the population. $\tilde{N}_c$ has a Poisson distribution with parameter $\tilde{\lambda} = N_c(x_{\max} - x_{\min})(y_{\max} - y_{\min})/ab$, in which N_c is the expected number of crystals per image, calculated from the PSD using

$$N_c = V_I \int_R^{L_{\max}} f(l)dl$$

The size of the local region surrounding the imaging volume is defined by $(x_{\min}, x_{\max}) = (-0.5\,\tilde{L}_{\max}, a + 0.5\,\tilde{L}_{\max})$ and $(y_{\min}, y_{\max}) = (-0.5\,\tilde{L}_{\max}, b + 0.5\,\tilde{L}_{\max})$ in which $\tilde{L}_{\max}$ equals $L_{\max}$ multiplied by the aspect ratio.

The particles generated by this stochastic process are projected onto the imaging plane as discussed previously.[13] The imaging parameters used in this study correspond to the specifications of a commercially available in situ video probe and are given in Table 2.

Results and Discussion

This section presents simulation results illustrating the capabilities and limitations of imaging based PSD measurement for industrial crystallization processes. First, we present the process and imaging simulation results for the batch crystallization process discussed in the previous section. Next, we analyze the data from these simulations to demonstrate the measurements obtainable by imaging. Specifically, we demonstrate both number- and weight-based PSD monitoring

Table 2. Parameters Used to Simulate Imaging of Particle Population Using Industrial Video Imaging Probe

Description	Symbol	Value
Horizontal dimension of imaging volume	a	1075 μm
Vertical dimension of imaging volume	b	850 μm
Depth of field	d	10 μm
Number of horizontal CCD pixels	$u_{\max}$	1360
Number of vertical CCD pixels	$v_{\max}$	1024
Micron-to-pixel ratio	m	0.8

as well as product quality measurements that are difficult to obtain using alternative monitoring technologies. We also discuss some of the limitations of current image analysis technology. Finally, we give general considerations for the design of imaging based PSD monitoring systems.

Process and imaging simulations

In previous studies of the photochemical system considered here, an optimal cooling profile was determined that minimized the ratio of the nucleus-grown and seed-grown crystal mass. The temperature and relative supersaturation profiles associated with the optimal cooling profile are compared against a linear cooling profile in Figure 1. This figure also shows the final weight PSDs resulting from the linear and optimal cooling profiles. The optimal profile uses high supersaturation at the beginning to maximize crystal growth. Despite the high supersaturation, secondary nucleation is negligible, because it depends not only on supersaturation but also on the amount of crystal mass present in the crystallizer. As the amount of crystal mass increases, the crystallizer is heated to reduce supersaturation and minimize secondary nucleation. The rapid cooling at the end of the batch results in both crystal growth and significant generation of nuclei, but the batch is terminated before these nuclei acquire appreciable mass.

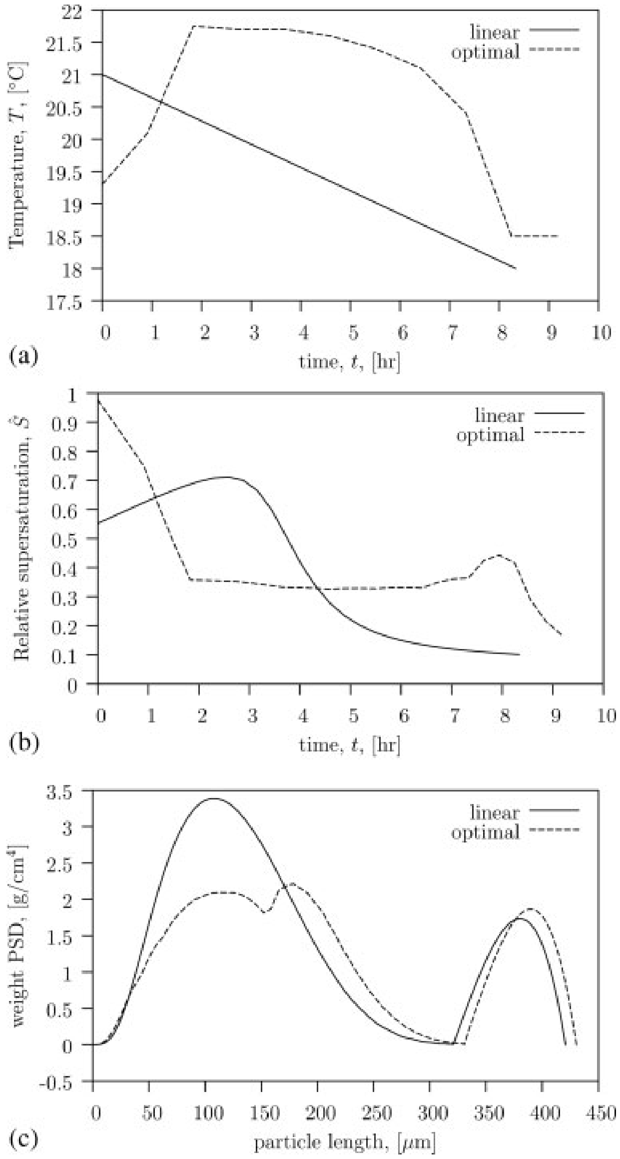

Figure 1. Comparison of simulation results for optimal and linear temperature trajectories.

(a) Temperature profiles. (b) Relative supersaturation profiles. (c) End-point PSDs (in terms of primary axis length).

Figures 2 and 3 show examples of artificial images corresponding to different times during the optimal and linear cooling processes. These artificial images simulate the images that would be obtained by a commercially available in situ video microscopy probe. Although real in situ images of the photochemical slurry are not available for comparison, Figure 4 shows real in situ images from a pharmaceutical crystallization involving crystals with a rod-like shape similar to that of the photochemical crystals. These real images highlight important similarities and differences with the simulated images. Like the simulated images, the particles in these real images appear to be randomly distributed throughout the image and exhibit a wide range of sizes while maintaining a similar high-aspect-ratio shape. The real particles' projected shapes are rectangular, similar to the projections in the simulated images. Although it is difficult to discern the true three-dimensional orientation of the particles using a two-dimensional image, the uniform degree of sharpness for each individual particle's outline suggests the particles are oriented essentially in a plane perpendicular to the camera's optical axis, similar to the orientation of the particles in the simulated images. On the other hand, the centroids of the particles in the simulated images are in a single plane, whereas the centroids of the particles in the real images appear to be in different planes, thus producing different degrees of sharpness between the outlines of different particles.

The primary difference between the simulated and real images is the contrast. Because the particles in the real image are illuminated using reflected light, the contrast between the particles and the background is poor. The simulated images have a perfect contrast, however, which is not attainable using reflected light but which may be nearly attainable using transmitted light and a narrow depth of field. Furthermore, the real images in Figure 4 contain significant background noise, particle texture, and motion blur. These effects are not included in the simulated images. Thus, we re-emphasize that the simulated images used in this study are idealized, but nonetheless useful for exploring the *limits* of what can be inferred using current camera hardware. We expect that

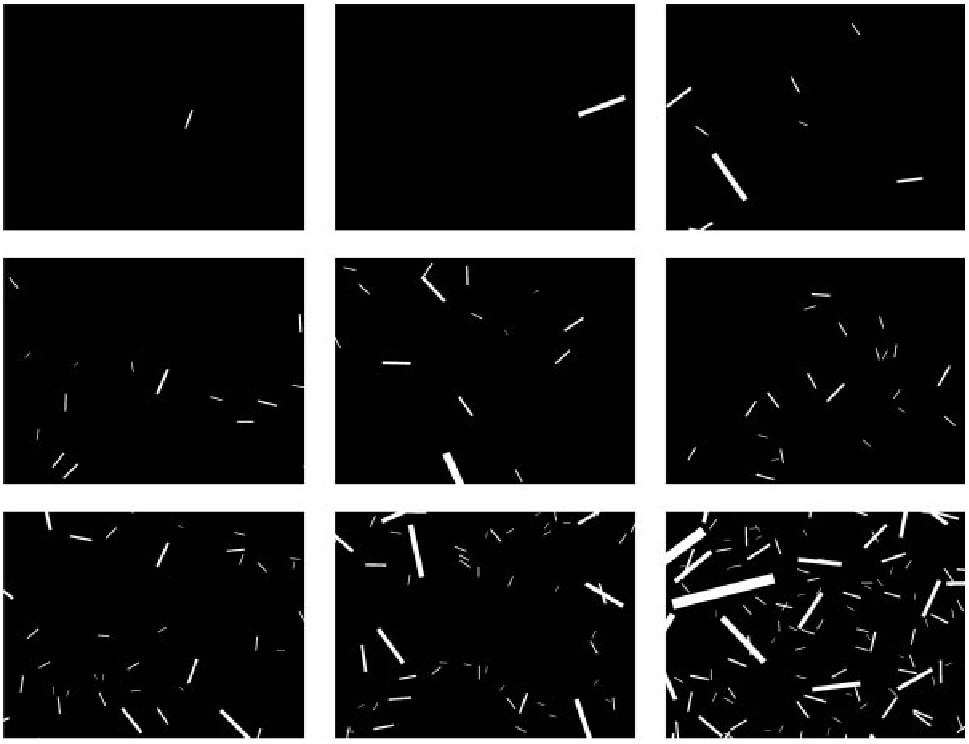

Figure 2. Examples of images generated at various times during the optimal cooling simulation.

The images correspond to 60-min intervals from 0 h (upper left) to 8 h (lower right).

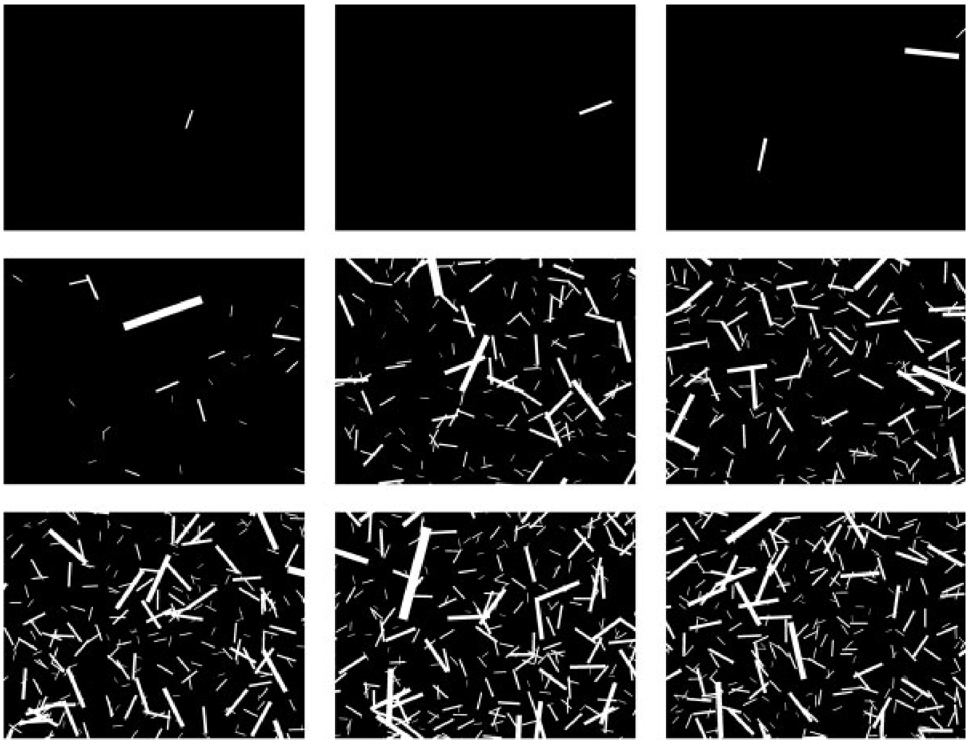

Figure 3. Examples of images generated at various times during the linear cooling simulation.

The images correspond to 60-min intervals from 0 h (upper left) to 8 h (lower right).

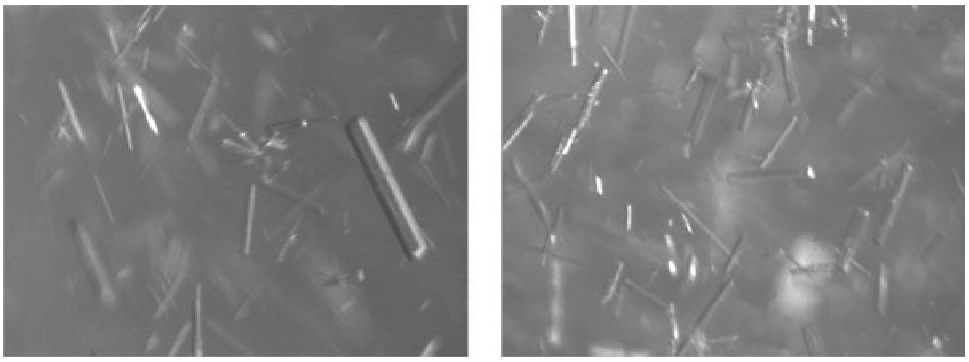

Figure 4. Examples of real in situ images of rod-like crystals.

continued improvements in the design of in situ video systems will lead to images that are increasingly similar to the idealized, simulated images used in this work.

Absolute PSD measurement

Figures 5 and 6 show, respectively, the number- and weight-based PSDs corresponding to the optimal cooling profile. The continuous curve shows the simulated PSD, and the histograms show the estimated PSD based on imaging measurements. These figures show that high-resolution (10 μm) PSD measurement is achievable using only 100 images.

Accurate PSD estimation requires not only sufficient sampling, but also effective image analysis. For example, Figure 6 indicates that, assuming perfect image analysis, 100 images provides sufficient samples to achieve a reasonably good estimate of the weight PSD for the given process conditions. Figure 7, on the other hand, shows the PSD estimated from image analysis data generated using the SHARC algorithm.[7] This figure indicates that towards the end of the experiment, the image analysis method identifies several false positives and also misses a significant number of both nucleus-grown crystals and seed-grown crystals. The failure of the image analysis algorithm is due to particle overlap. Different image

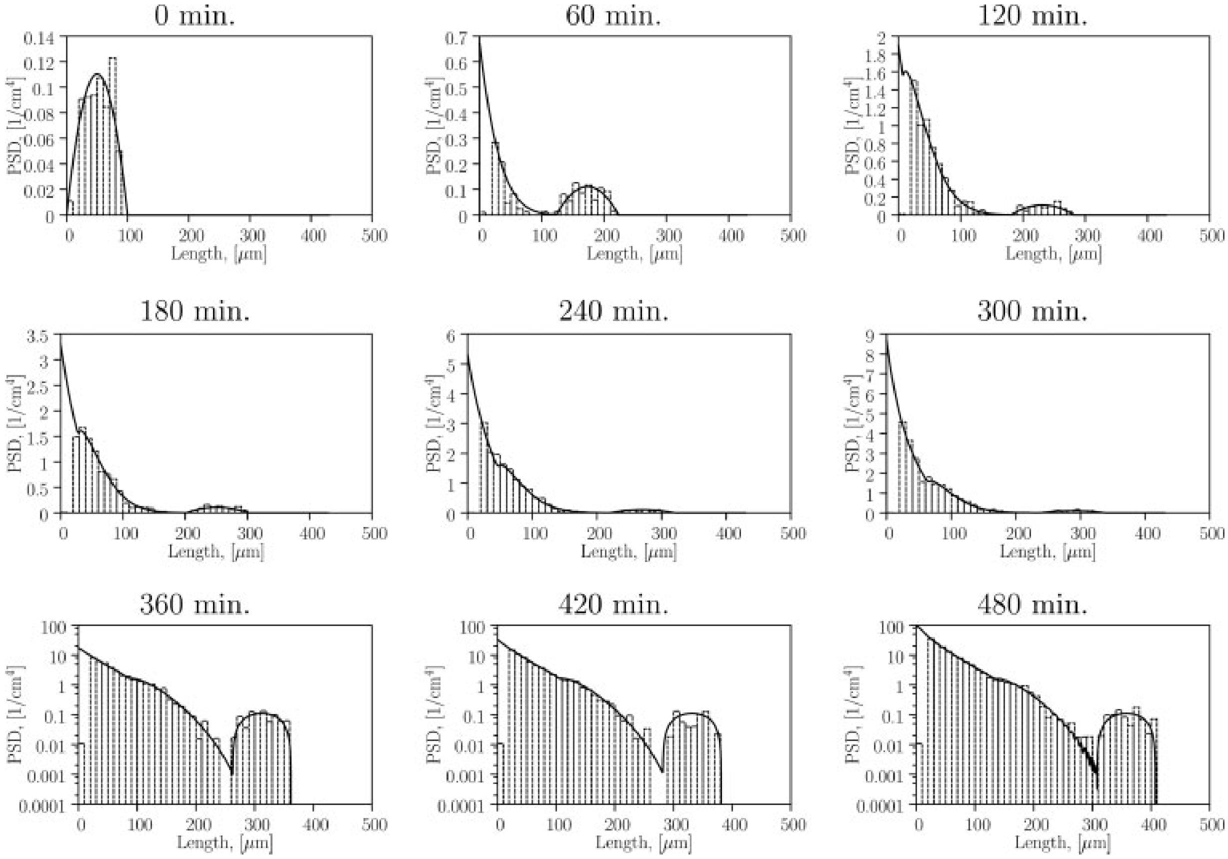

Figure 5. Evolution of measured and estimated number-based PSD for optimal cooling and perfect image analysis.

Snapshots shown from $t = 0$ min to $t = 480$ min at 60 min intervals. Bin size = 10 μm and $N = 100$.

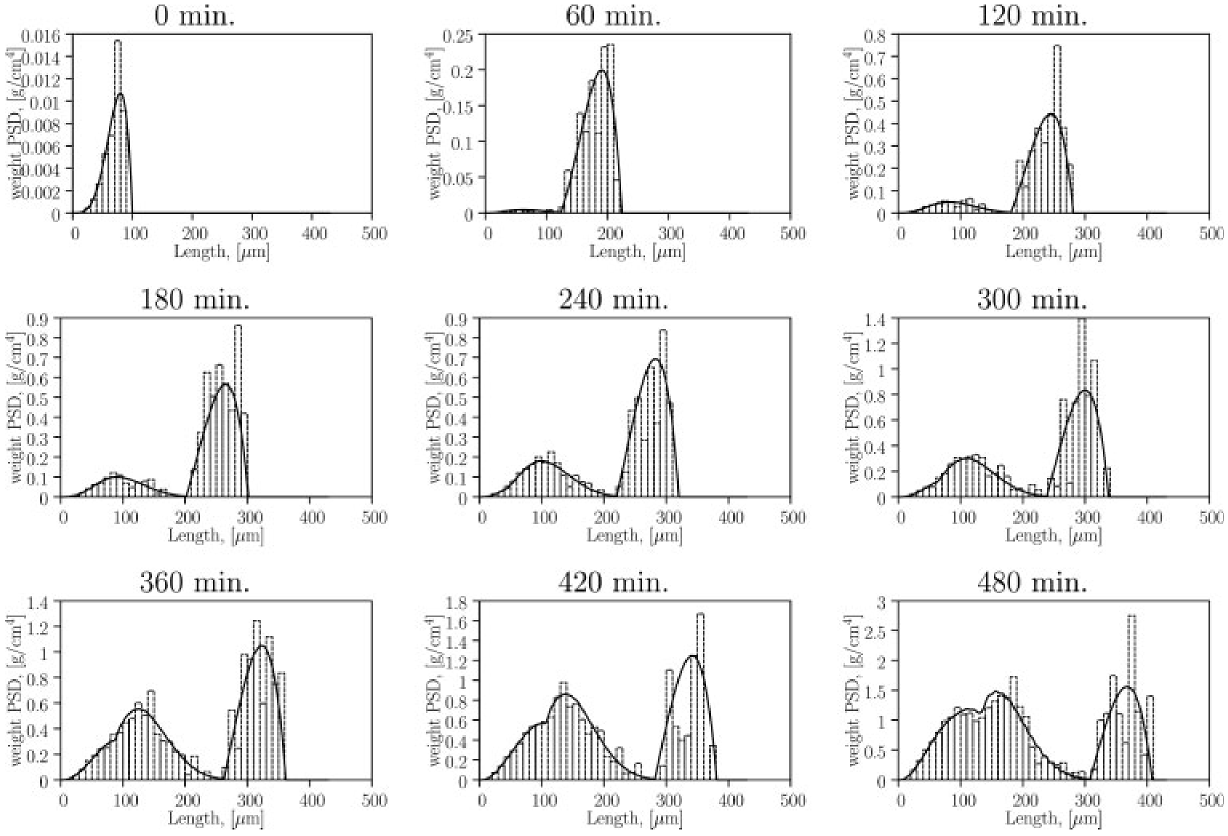

Figure 6. Evolution of measured and estimated weight PSD for optimal cooling and perfect image analysis.

Snapshots shown from $t = 0$ min to $t = 480$ min at 60 min intervals. Bin size = 10 μm and $N = 100$.

analysis algorithms have different tolerances for overlap, with model-based algorithms typically tolerating more overlap than other methods. On the basis of the images in Figure 2, one could reasonably expect improvements in model-based image analysis algorithms to enable effective measurement for almost the entire duration of the process. On the other hand, particle overlap can be so excessive for some systems that effective image analysis is unachievable.

Measurements for product quality

Product quality is often assessed based on the PSD. A variety of product quality metrics are used in the crystallization optimal control literature (see Ward et al.[18]). The metrics involve both lower (number-based) and higher (weight-based) moments of the PSD, as well as moments specific to the seed-grown crystals and nucleus-grown crystals. In the following, we demonstrate the feasibility of monitoring a variety of these metrics using imaging.

Ratio of nuclei mass relative to seed mass

The ratio of nucleus-grown crystal mass m_N to seed-grown crystal mass m_S affects the efficiency of downstream filtration processes.[16,19] For the photochemical system considered here, $m_N/m_S = \mu_{N_3}/\mu_{S_3}$ cannot be measured using conventional technologies. The needle-like shape violates the sphericity assumption necessary for effective PSD measurement by light scattering and also complicates mechanical sieving. In previous studies of this system, these measurement difficulties motivated the use of scanning electron and optical microscopy to characterize the PSD qualitatively in terms of habit and maximum size.[15] Quantitative PSD measurement by microscopy could not be achieved because of sampling limitations. Using high-speed, in situ video microscopy, however, a sufficient number of samples can be obtained to enable measurement of m_N/m_S.

In both cases, the images contain sufficient particles to enable estimation of m_N/m_S, as shown in Figure 8. The estimates of m_N/m_S shown in Figure 8 are based on a sample size of 100 images, corresponding to a sample time of approximately 3 s (assuming the standard 30 frames/second acquisition rate). The m_N/m_S estimates are also based on the assumption that every particle appearing completely inside the imaging volume (not touching any borders) is identified perfectly.

Mean crystal size and coefficient of variation

The mean crystal size is commonly reported as an indication of product quality. Both the number-based mean size (μ_1/μ_0) and weight-based mean size (μ_4/μ_3) can be estimated effectively using imaging-based measurement, as shown in Figure 9.

The coefficient of variation c_v quantifies the distribution spread. Typically a small c_v is desired to improve the efficiency of downstream manufacturing processes. Figure 10 demonstrates that both the number-based c_v ($\mu_2\mu_0/\mu_1^2$) and

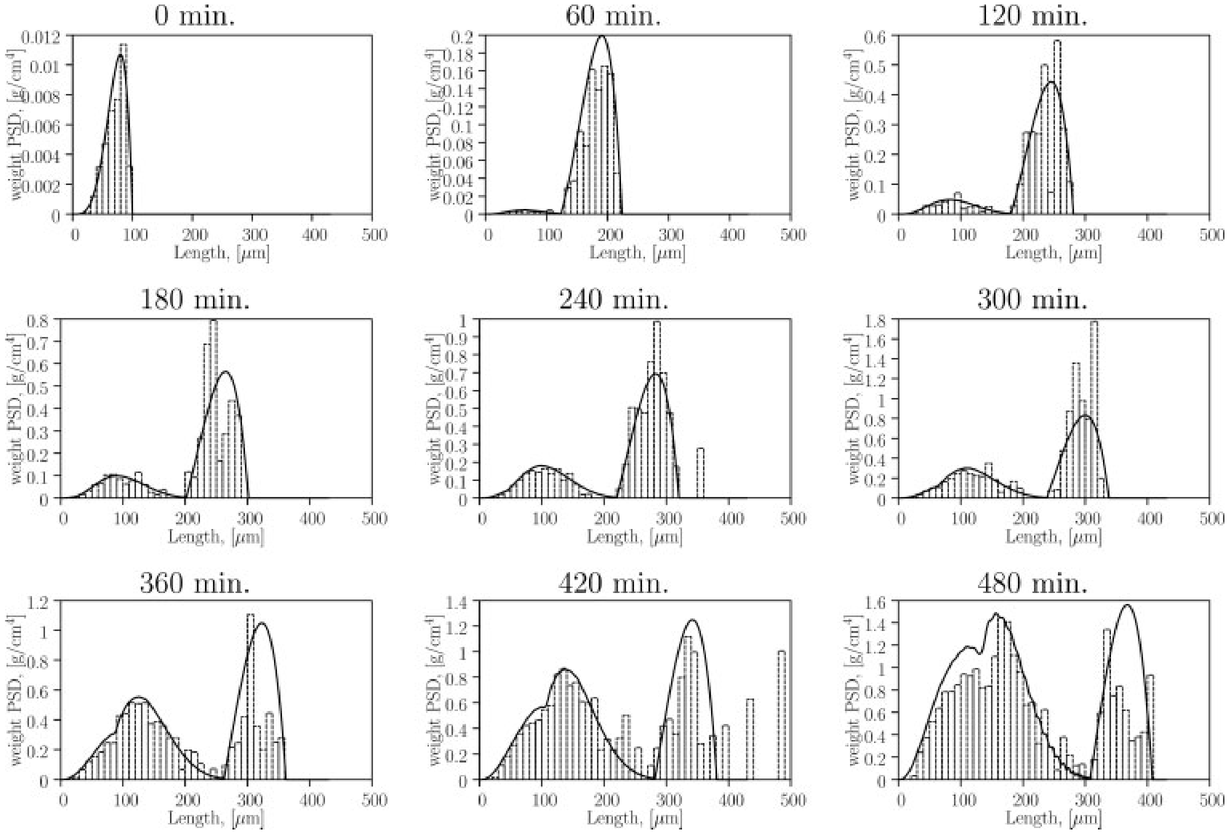

Figure 7. Evolution of measured and estimated weight PSD for optimal cooling and image analysis using SHARC.

Snapshots shown from $t = 0$ min to $t = 480$ min at 60 min intervals. Bin size $= 10$ μm and $N = 100$.

weight-based c_{v_w} ($\mu_5\mu_3/\mu_4^2$) can be measured effectively by imaging.

General imaging considerations

The previous section demonstrated the feasibility of high-resolution PSD measurement for a specific, industrial crystallization process and realistic imaging conditions. This section discusses general sampling and image analysis considerations for imaging based PSD measurement.

Sampling

A fundamental problem for imaging based PSD monitoring is determining the number of images to acquire. The problem is nontrivial, because the answer depends not only on the desired accuracy, but also on the way in which the histogram is binned, the imaging conditions, and on the PSD itself. Many of the imaging related articles cited previously discuss the number of samples required for their specific system. Here, we propose some general guidelines applicable to imaging of particulate processes in general.

Previously, we proposed a methodology for constructing confidence intervals for an imaging based PSD measurement.[13] The methodology provides a framework for determining the number of images necessary to achieve a desired accuracy. Number-based PSDs are typically measured by discretizing the characteristic length scale into T nonoverlapping bins or size classes. We therefore define the discrete PSD as

$$\rho_i = \int_{S_i}^{S_{i+1}} f(l)dl, \quad i = 1, \ldots, T \tag{7}$$

in which $\mathbf{S} = (S_1, \ldots, S_{T+1})$ is the vector of breaks between size classes. The maximum likelihood estimate of ρ_i is calculated from imaging data using

$$\hat{\rho}_i = \frac{X_i}{N\alpha_i} \tag{8}$$

in which X_i is the total number of particles observed in N images with lengths corresponding to bin i, and α_i is a scalar

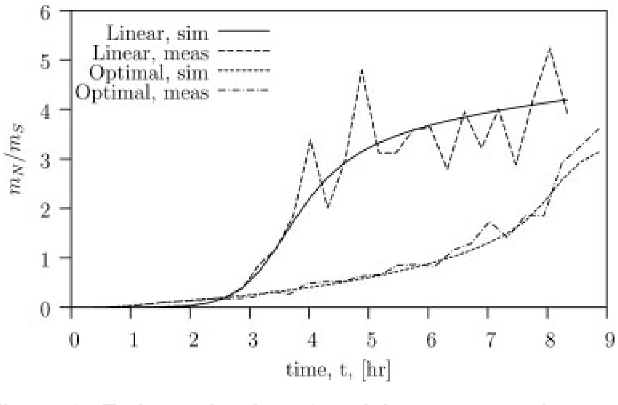

Figure 8. Estimated ratios of nuclei mass to seed crystal mass for optimal and linear cooling for $N = 100$.

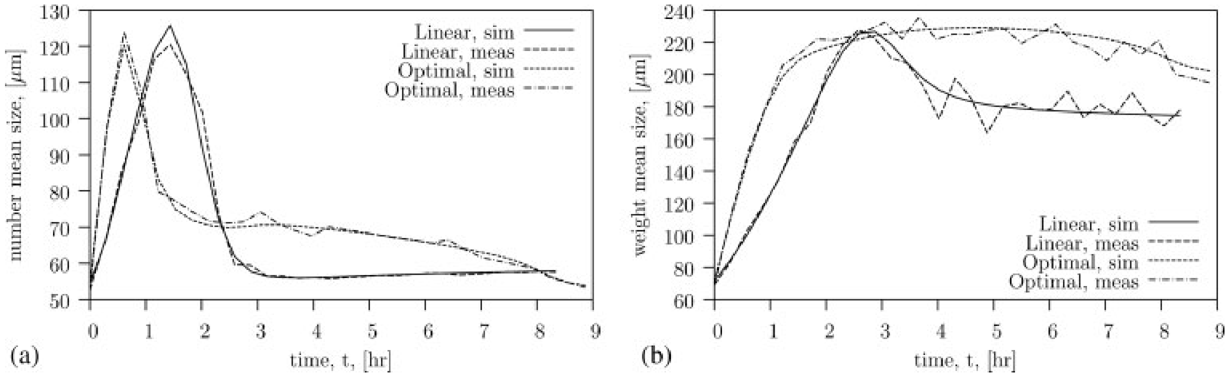

Figure 9. Estimated mean crystal sizes for optimal and linear cooling, $N = 100$.

(a) Number-based. (b) Weight-based.

that corrects for edge effects due to the finite size of the imaging frame (α_i approaches 1 for infinitely small particles and approaches 0 for particles the size of the image field of view). The variance of this estimator, which is directly related to the confidence intervals, is given by

$$Var(\hat{\rho}_i) = \frac{\rho_i}{N\alpha_i} \tag{9}$$

Equation 9 contains all the process, imaging, and sampling information necessary to assess the accuracy of an imaging based PSD measurement. As mentioned, the accuracy depends not only on the number of images N and the desired resolution, but also on the imaging conditions, particle size, particle geometry (all of which are encapsulated in the correction factor α_i), and on the number density of particles ρ_i. As a result, the number of images required to obtain a given accuracy changes as the particle population evolves.

To use Eq. 9, one needs to know ρ_i. Batch crystallizations are typically seeded, and usually some knowledge of the seed population is available. For example, if the seed crystal population is prepared by sieving, the initial minimum crystal size and maximum size are known. The mass of seed crystals injected into the crystallizer is also known. This information is sufficient to obtain a rough estimate of ρ_i for the bins corresponding to the seed population, enabling calculation of the N that gives a sufficiently small variance (i.e., confidence interval). It is, of course, desirable to monitor the PSD of the nucleus-grown crystals also, but the number of the nucleus-grown crystals typically is much greater than the number of the seed-grown crystals, as illustrated in Figure 5. Thus, from a sampling standpoint, a sample size N that provides sufficient accuracy relative to seed PSD properties can be expected to provide sufficient accuracy relative to the PSD properties of the nucleated crystals, which are both smaller and (usually) more numerous than the seeds.

Image analysis

Imaging based PSD measurement requires not only sufficient sampling but also effective image analysis. The effectiveness of any image analysis algorithm depends strongly on the amount of particle overlap. An approach for quantifying the amount of particle overlap for monodisperse populations has been introduced previously.[14,20,21] With this approach, the average number of overlaps per particle is predicted to be

$$D = \mu_0 \Omega d \tag{10}$$

in which D is the average number of overlaps, μ_0 is the zeroth moment of the PSD, d is the depth of field, and Ω is the "admissible area," which is based on the particle geometry. Assuming random orientation in the plane perpendicular to the camera's optical axis, Ω is calculated using Mack's formula[20]:

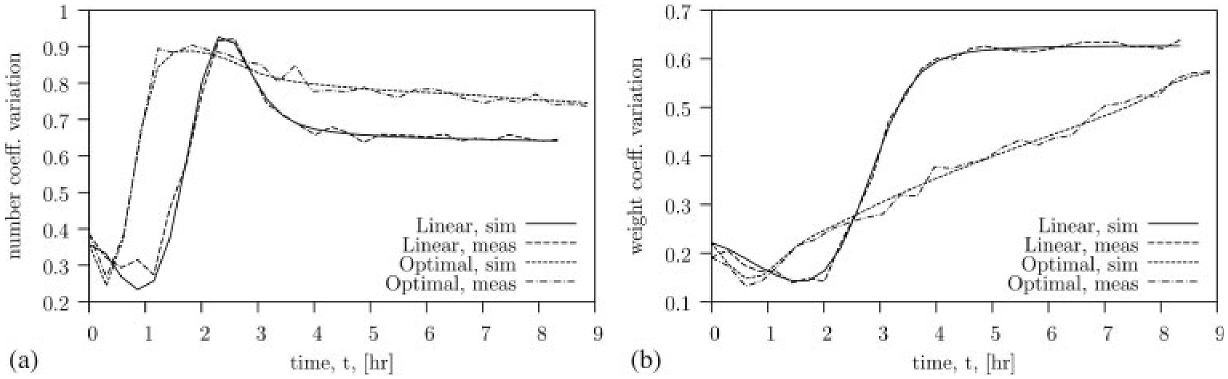

Figure 10. Estimated coefficients of variation for optimal and linear cooling, $N = 100$.

(a) Number-based. (b) Weight-based.

$$\Omega = 2a_p + \frac{s_p^2}{2\pi} \tag{11}$$

in which a_p and s_p are, respectively, the projected area and perimeter of a single particle in its preferred (resting) orientation. This equation can be used to show, for example, that as the aspect ratio of the particles increases, the solid concentration at which acceptable image processing can be achieved decreases. Equation 10 can be used to determine appropriate sampling conditions for imaging-based measurement. For example, one could assume the seed population to be approximately monodisperse and use Eq. 10 to predict the number of overlaps per particle for a given mass of seed. If the number of overlaps is too high for current image analysis methods, one may choose to use dilution or an optical system with a smaller depth of field.

Conclusion

Video imaging is a viable technology for on-line PSD monitoring and control. The feasibility of high-resolution, imaging based PSD measurement has been demonstrated using a realistic industrial crystallization process. Imaging based measurement enables both number- and weight-based PSD monitoring as well as product quality measurements that are difficult to obtain using alternative monitoring technologies, such as the ratio of nuclei mass to seed mass. Although the images used in this study are idealized and do not reflect all the challenges of real images, the results nonetheless indicate that a single, high-resolution camera with large field of view can track adequately both the nucleated crystal population and seed crystal population. The results also show that current camera hardware enables acquisition of sufficient samples to enable accurate PSD estimation in a reasonable amount of time. General recommendations for determining appropriate sampling conditions for imaging based PSD measurement have also been given. The proposed tools facilitate the design of effective, imaging based PSD monitoring technology.

This article has also highlighted directions for future research to improve imaging based PSD measurement. Most importantly, advances in image analysis algorithms are needed to improve image segmentation when particle overlap is significant. These advances will require further statistical estimation studies to address sampling biases due to particle overlap or occlusion. Although effective statistical methods have been developed to address two-dimensional edge effects (i.e., sampling bias associated with the finite size of the imaging window), further consideration is required for errors associated with three-dimensional depth of field effects (i.e., sampling bias associated with the finite size of the imaging depth).

Acknowledgments

This material is based upon work supported by the National Science Foundation under Grant No. 0540147.

Literature Cited

1. Schöll J, Bonalumi D, Vicum L, Mazzotti M, Müller M. In situ monitoring and modeling of the solvent-mediated polymorphic transformation of L-glutamic acid. *Crystal Growth Design*. 2006;6:881–891.
2. Monnier O, Fevotte G, Hoff C, Klein JP. Model identification of batch cooling crystallizations through calorimetry and image analysis. *Chem Eng Sci*. 1997;52:1125–1139.
3. Pöllänen K, Häkkinen A, Reinikainen S-P, Louhi-Kultanen M, Nyström L. A study on batch cooling crystallization of sulphathiazole: process monitoring using ATR-FTIR and product characterization by automated image analysis. *Chem Eng Res Design*. 2006;84:47–59.
4. Patience DB, Dell'Orco PC, Rawlings JB. Optimal operation of a seeded pharmaceutical crystallization with growth-dependent dispersion. *Organic Process Res Develop*. 2004;8:609–615.
5. Calderon De Anda JA, Wang XZ, Lai X, Roberts KJ. Classifying organic crystals via in-process image analysis and the use of monitoring charts to follow polymorphic and morphological changes. *J Process Control*. 2005;15:785–797.
6. Dharmayat S, Calderon De Anda J, Hammond RB, Lai X, Roberts KJ, Wang XZ. Polymorphic transformation of L-glutamic acid monitored using combined on-line video microscopy and X-ray diffraction. *J Crystal Growth*. 2006:294:35–40.
7. Larsen PA, Rawlings JB, Ferrier NJ. An algorithm for analyzing noisy, in situ images of high-aspect-ratio crystals to monitor particle size distribution. *Chem Eng Sci*. 2006;61:5236–5248.
8. Larsen PA, Rawlings JB, Ferrier NJ. Model-based object recognition to measure crystal size and shape distributions from in situ video images. *Chem Eng Sci*. 2007;62:1430–1441.
9. Qu H, Louhi-Kultanen M, Kallas J. In-line image analysis on the effects of additives in batch cooling crystallization. *J Crystal Growth*. 2006;289:286–294.
10. Watano S, Miyanami K. Image processing for on-line monitoring of granule size distribution and shape in fluidized bed granulation. *Powder Technol*. 1995;83:55–60.
11. Blandin A-F, Rivoire A, Mangin D, Klein J-P, Bossoutrot J-M. Using in situ image analysis to study the kinetics of agglomeration in suspension. *Particle Particle Syst Character*. 2000;17:16–20.
12. Hukkanen EJ, VanAntwerp JG, Braatz RD. Determination of breakage and coalescence kinetics in suspension polymerization reactors using in-situ laser backscattering and process video microscopy. Submitted to *Chem Eng Sci*. 2007.
13. Larsen PA, Rawlings JB. Maximum likelihood estimation of particle size distribution for high-aspect-ratio particles using in situ video imaging. Submitted to *Technometrics*. 2007. See also Ref. 17. pp. 95–112.
14. Larsen PA, Rawlings JB. Assessing the reliability of particle size distribution measurements obtained by image analysis. Accepted for publication in *Particle Particle Syst Character*. 2007.
15. Matthews HB. Model Identification and Control of Batch Crystallization for an Industrial Chemical System. PhD thesis, University of Wisconsin–Madison, 1997.
16. Matthews HB, Rawlings JB. Batch crystallization of a photo chemical: Modeling, control and filtration. *AIChE J*. 1998;44:1119–1127.
17. Larsen PA. Computer Vision and Statistical Estimation Tools for in situ, Imaging-Based Monitoring of Particulate Populations. PhD thesis, University of Wisconsin–Madison, 2007. Available at http://jbrwww.che.wisc.edu/theses/larsen.pdf
18. Ward JD, Mellichamp DA, Doherty MF. Choosing an operating policy for seeded batch crystallization. *AIChE J*. 2006;52:2046–2054.
19. Jones AG, Budz J, Mullin JW. Batch crystallization and solid-liquid separation of potassium sulphate. *Chem Eng Sci*. 1987;42:619–629.
20. Mack C. The expected number of clumps when convex laminae are placed at random and with random orientation on a plane area. *Proc Cambridge Philos Soc*. 1954;50:581–585.
21. Roach SA. *The Theory of Random Clumping*. Methuen's monographs on applied probability and statistics. London: Methuen & Company; 1968.

Manuscript received Jun. 29, 2007, and revision received Sept. 22, 2008.